Directional scattering and multipolar contributions to optical forces on silicon nanoparticles in focused laser beams

Research Article | Vol. 26, No. 22 | 29 Oct 2018 | OPTICS EXPRESS 29074
Optics EXPRESS

Directional scattering and multipolar contributions to optical forces on silicon nanoparticles in focused laser beams

NILS ODEBO LÄNK,[1,3] PETER JOHANSSON,[1,2] AND MIKAEL KÄLL[1,4]

[1] *Department of Physics, Chalmers University of Technology, 412 96 Göteborg, Sweden*
[2] *School of Science and Technology, Örebro University, 701 82 Örebro, Sweden*
[3] *odebo@chalmers.se*
[4] *mikael.kall@chalmers.se*

Abstract: Nanoparticles made of high index dielectric materials have seen a surge of interest and have been proposed for various applications, such as metalenses, light harvesting and directional scattering. With the advent of fabrication techniques enabling colloidal suspensions, the prospects of optical manipulation of such nanoparticles becomes paramount. High index nanoparticles support electric and magnetic multipolar responses in the visible regime and interference between such modes can give rise to highly directional scattering, in particular a cancellation of back-scattered radiation at the first Kerker condition. Here we present a study of the optical forces on silicon nanoparticles in the visible and near infrared calculated using the transfer matrix method. The zero-backscattering Kerker condition is investigated as an avenue to reduce radiation pressure in an optical trap. We find that while asymmetric scattering does reduce the radiation pressure, the main determining factor of trap stability is the increased particle response near the geometric resonances. The trap stability for non-spherical silicon nanoparticles is also investigated and we find that ellipsoidal deformation of spheres enables trapping of slightly larger particles.

1. Introduction

Optical trapping of non-resonant dielectric particles dates back almost 50 years [1]. Since then, trapping and manipulation of such particles in optical tweezers has opened up a wealth of opportunities in biology and biotechnology [2, 3]. Typical particles of this type are made of latex (polystyrene) or glass, with refractive index n around 1.4–1.6. Trapped biological matter, such as cells, also fall within this refractive index range. Trapping of metallic nanoparticles with localized surface plasmon resonances (LSPRs) in the visible region is also the subject of considerable interest for various applications [4], including biomolecular [5] and cellular [6] analysis, photothermal imaging [7], novel lithography methods [8] as well as more basic studies such as non-equilibrium thermodynamics [9], to name a few.

Particles that are resonant at a wavelength close to the trapping wavelength inevitably exhibit significant light extinction. This enhanced scattering and absorption amplifies the momentum transfer from the beam to the particle and strongly influences the 3D stability of a single-beam optical trap, since the axial restoring force has to overcome the resonant forward momentum transfer for the trap to be stable. In a dipole approximation, this corresponds to axial gradient forces overcoming radiation pressure forces in the direction of the incident laser beam. This is difficult to achieve in practice, and trapping of resonant particles is therefore typically done only in the two lateral dimensions, using electrostatic repulsion from a surface to counteract the radiation pressure in the third direction [6, 10], or by using two counter-propagating beams [1, 11]. This constrains the utility of the optical tweezers and makes it more difficult to move the particle to a specific location.

High index dielectric (HID) nanoparticles have been demonstrated to be a competitive

#341758 https://doi.org/10.1364/OE.26.029074
Journal © 2018 Received 7 Aug 2018; revised 24 Sep 2018; accepted 24 Sep 2018; published 24 Oct 2018

Optics EXPRESS

alternative to resonant metal nanoparticles in, for example, the design of metasurfaces [12–14] and optical or optoelectronic devices [15–17]. Because of the high refractive index, $n > \sim 3$, HID nanoparticles support geometric resonances of electric and magnetic character in the visible and near infra-red spectral range, where optical absorption is low [18, 19]. This is in contrast to plasmonic nanoparticles, which always exhibit significant absorption due to Ohmic losses. The potential to exploit these properties has made optical trapping and manipulation of HID nanoparticles an interesting line of research. Examples include optical sorting [20], optical binding forces [21] and recent experimental demonstrations [22].

Interference between different multipolar modes in HID particles can give rise to highly directional scattering [23–25]. In particular, interference between electric and magnetic dipole scattering can result in complete cancellation of backscattered light. This is known as the first Kerker condition [26] and can be realized in high index dielectric spheres [24, 27]. Multipolar interference effects have been discussed as a necessity for the realization of an optical pulling force, or tractor beam, where one diffractionless optical beam [28, 29] or two beams at an angle [28, 30] are used to realize a negative force over a macroscopic distance. For the case of plane wave illumination and passive materials, it is impossible to realize a pulling force regardless of particle specifics [29]. It has however been suggested that complete suppression of backscattered radiation can serve to reduce the momentum transfer from the beam to the particle and thus give rise to a more stable trap [28, 31].

While the first Kerker condition has been discussed previously with regard to radiation pressure for silicon particles in a plane wave [32, 33], no study on these effects in the case of optical tweezers, that is, a single focused Gaussian laser beam, have been published, to the best of our knowledge. Previous studies have been made on how Mie resonances of dielectric particles affect optical forces in a focused beam [34, 35]; however, these studies consider larger particles with a low to moderate refractive index ($n < 2$).

In this work, we investigate the optical forces on silicon nanospheres, the prototypical example of a HID nanoparticle, for realistic optical tweezer parameters in order to evaluate how asymmetric scattering (in the forward-backward sense) and the first Kerker condition influences optical trap stability. First, we study the case of plane wave excitation of a silicon sphere in water in order to examine how this scattering asymmetry affects the optical forces in the presence of radiation pressure only. Next, to understand the interference effects and multipolar contributions in a realistic optical tweezer experiment, we study how illumination by a focused Gaussian laser beam deviates from the plane wave behaviour. Moreover, we use symmetry to separate the gradient forces from the radiation pressure and discuss the multipolar contributions to each component. Since optimal forward-to-backward scattering ratios are not found in spherical high-index particles but rather in ellipsoidal shapes [36, 37], we finally investigate the optical trap stability for deformed silicon spheres.

2. Results and discussion

The electrodynamics simulations used here for calculating the optical forces consist of either a plane wave or a focused laser beam in an angular spectrum representation [38]. This means that the electromagnetic fields exciting the nanoparticle are not paraxial but are true solutions to the Maxwell equations. The incident fields are projected, through numerical integration, onto vector spherical harmonics on the surface of a sphere, S_c , circumscribing the nanoparticle. The response of the particle is then calculated through the Transfer Matrix approach [39] and is expanded into electric and magnetic multipole fields on the circumscribing sphere. The optical properties can then be calculated in the Mie theory framework. The time-averaged optical force, for example, is obtained by integration of the outward normal component of the Maxwell stress

Optics EXPRESS

tensor, $\overleftrightarrow{T}$ [40, 41]

$$\langle \vec{F} \rangle = \langle \int_{S_c} \hat{n} \cdot \overleftrightarrow{T} \, \mathrm{d}S \rangle , \tag{1}$$

which can be easily performed with the aid of the Wigner-Eckart theorem [41] since the fields are expressed in a series of spherical multipole terms. In the present case, the full T-matrix approach is preferred above the more transparent analytical point dipole approximations commonly found in optical tweezer literature since the particle response is beyond dipolar for larger sizes. All calculations were performed assuming a uniform aqueous surrounding medium (n_s = 1.33).

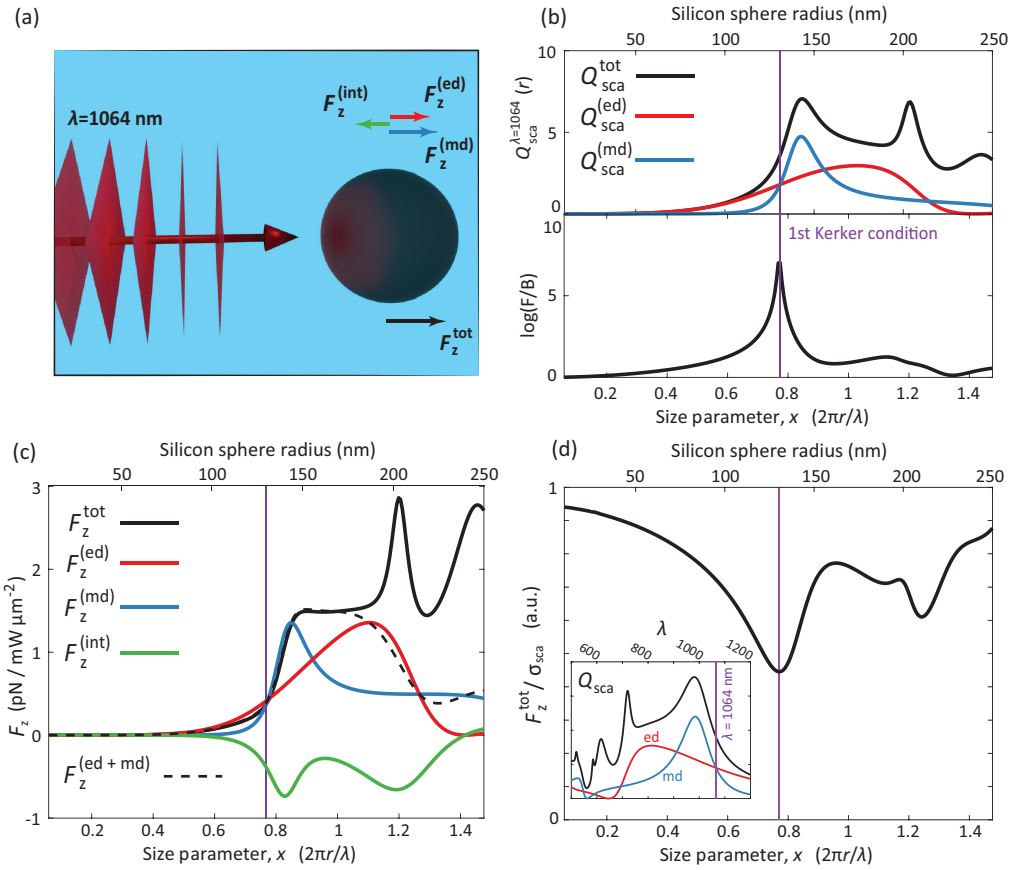

Fig. 1. Silicon spheres subject to λ = 1064 nm plane wave excitation. (a) Schematic of the system. (b) Scattering efficiency and forward-to-backward scattering ratio versus size-parameter x, showing the well-known divergence at the first Kerker condition (x_k = 0.776, r_k = 131 nm). (c) Radiation pressure force on Si spheres in a plane wave (full black line) versus x, together with the pure electric (red) and magnetic dipole (blue) forces and the contribution from their interference (green), respectively. Note that the interference contribution decreases the radiation pressure, but the effect is strongest a higher radius than the first Kerker condition. The dashed curve in (c) shows that the sum of the two dipolar contributions completely dominates the radiation pressure force up until slightly above x = 1 where the magnetic quadrupole starts playing a role. (d) The total radiation pressure force normalized by the scattering cross section of the particle, demonstrating that the first Kerker condition is the optimal angular distribution of scattered radiation. The inset shows the scattering efficiency versus wavelength for a Si sphere in water with radius r_k = 131 nm, fulfilling the first Kerker condition at λ = 1064 nm.

Optics EXPRESS

2.1. Plane wave excitation

First, we revisit the well-known case of plane wave excitation [Fig. 1]. This will reveal the multipolar interaction and the role of the first Kerker condition in the presence of radiation pressure only. We fix the wavelength of the incident radiation to $\lambda = 1064$ nm, the most common laser wavelength in optical tweezers technology, and instead vary the particle size and, thus, the size parameter ($x = 2\pi r/\lambda$). The complex refractive index of crystalline silicon at this wavelength is $n = 3.55 + i0.000083$ [42] but, since the dispersion $n(\lambda)$ is weak in the visible to near-infrared spectral region, results obtained for a particular x at $\lambda = 1064$ nm can be used also for neighboring trapping wavelengths with good accuracy.

We note that the optical absorption of Si at 1064 nm is very small (well below 0.2% of the extinction for particle sizes above $r \approx 40$ nm) since the photon energy of the incident light is just slightly larger than the indirect band gap of Si, corresponding to $\lambda \approx 1150$ nm. As a consequence, the radiation pressure is completely dominated by scattering and while absorption is included in the calculations, it will not be further discussed.

The characteristic hallmarks of the first Kerker condition can be seen in the scattering properties as a function of size parameter x in Fig. 1. We decomposed the scattered power into electric dipole and magnetic dipole contributions [Fig. 1(b)], which can be done since interference between different multipoles does not affect the total power scattered in each multipolar channel. The peak in scattering at around $x = 1.2$ is due to the magnetic quadrupole and is therefore absent from both the electric and magnetic dipole contributions. The first Kerker condition occurs at the crossing of the electric and magnetic dipole resonances, where these dipole excitations are of equal magnitude and are in phase [26]. When this condition is fulfilled, we see a spike in the forward-to-backward scattering ratio [shown in logarithmic scale in Fig. 1(b)], defined as $F/B = \frac{\mathrm{d}\sigma_s}{\mathrm{d}\Omega}\big|_{\theta=0^\circ} / \frac{\mathrm{d}\sigma_s}{\mathrm{d}\Omega}\big|_{\theta=180^\circ}$, where $\frac{\mathrm{d}\sigma_s}{\mathrm{d}\Omega}$ is the differential scattering cross-section. This is due to a complete cancellation of backscattered radiation due to perfect destructive interference in the backward direction, $\theta = 180^\circ$. For $\lambda = 1064$ nm, the first Kerker condition is fulfilled for a Si sphere of radius $r_\mathrm{k} = 131$ nm. A scattering spectrum for a Si sphere with this radius is shown as an inset in Fig. 1(d). One might expect that the highly forward-directed scattering should give rise to a reduction in the momentum transferred from the beam to the particle. In fact, considering the particle as a simple source of scattered radiation would give rise to a negative radiation pressure force, since the scattering is predominantly directed in the forward half-space. However, when also considering the incident field, it is clear that no net attractive force can be achieved since any scattering of the incident plane wave photons by the particle can only reduce their forward momentum or, at best, leave it unchanged. The momentum lost by the incident field is transferred to the particle, therefore inducing a force in the forward direction.

In the dipole approximation for magneto-electric particles in a plane wave, one typically decomposes the radiation pressure force into three contributions [43], namely

$$F^{\mathrm{tot}} = F^{(\mathrm{ed})} + F^{(\mathrm{md})} + F^{(\mathrm{int})}\,, \tag{2}$$

where $F^{(\mathrm{ed})}$ is the force on the particle stemming from its electric dipole polarizability and likewise for $F^{(\mathrm{md})}$, from the magnetic dipole polarizability. In contrast to the scattered power, the radiation pressure force contains a cross term due to the interference between the scattering from the electric and the magnetic dipoles. This term can become negative and thus serve to reduce the radiation pressure by means of coherent interaction between electric and magnetic dipole excitations. In order to decompose the force according to Eq. (2), we first calculated the multipolar response of the sphere. Then, in the calculations of the optical force, we used only a single dipolar Mie response coefficient at a time, with the rest set to zero. The dipole interference force was then obtained through $F^{(\mathrm{int})} = F^{(\mathrm{ed+md})} - F^{(\mathrm{ed})} - F^{(\mathrm{md})}$, where $F^{(\mathrm{ed+md})}$ corresponds to the force when both electric and magnetic dipolar coefficients are included [black dashed line in Fig. 1(c)].

Optics EXPRESS

As is clear from a comparison of the spectral profiles in Fig. 1(b) and (c), the interference force, $F^{(\mathrm{int})}$, does not exhibit a minimum at the first Kerker condition, as one might expect, but rather at slightly larger particle sizes. This behavior, which can be seen but is not discussed in [32], demonstrates that momentum transfer is not straightforwardly related to the forward-to-backward scattering ratio. The reason that the interference force is not minimized at the first Kerker condition is that the stronger particle response closer to the dipolar resonance peaks amplifies the total scattered power, and thus the interference force. To demonstrate this, we normalized the total radiation pressure force, F_z^{tot}, by the scattering cross section, σ_s [Fig. 1(d)] in order to decouple the total particle response from the angular distribution of the scattered radiation. We then see that the first Kerker condition does correspond to the optimal angular distribution in terms of minimum momentum transfer.

2.2. Optical forces in a focused Gaussian beam

Guided by the insights discussed above, we now turn to the question of how the asymmetric scattering from a Si particle affects the possibility to trap the particle using a single focused laser beam. We confine ourselves to studying the optical forces acting in the light propagation direction, since these are the forces that limit the three-dimensional stability of a single-beam laser trap. Specifically, we investigate whether the interference forces in the radiation pressure, aided by restoring forces that arise due to field intensity gradients near a tight focus, can overcome the forward momentum transfer. Moreover, we explore whether multipolar interference affects these restoring forces. To this end, we calculated the optical force for varying particle position along the optical axis for a tightly focused laser beam in the angular spectrum representation [38]. As above, we fixed the trapping wavelength at $\lambda = 1064$ nm and used a surrounding medium of water. We studied the stability of the optical trap for a silicon sphere of size parameter $x^* = 0.737$ (radius $r^* = 124.8$ nm), since this turns out to be the size at which the trap is most stable [Fig. 3]. Circular polarization of the incident light is used throughout. While unimportant for spherical particles, the choice of polarization will be significant when we consider anisotropic particles in Sec. 2.3. These parameters, along with our chosen objective numerical aperture of NA = 1.2, constitute realistic and typical experimental conditions for optical tweezer research. The numerical aperture sets the beam focus width by fixing the maximum angle of convergence through $\mathrm{NA} = n_{\mathrm{s}} \sin \alpha_{\max}$ and our chosen NA results in a beam waist radius of $w = 407$ nm (where the intensity has dropped to $1/\mathrm{e}^2$ of its axial value). The results of this analysis are summarized in Fig. 2.

In the electric dipole approximation and for a properly radiation-corrected electric dipole polarizability α_{e}, the optical force can be decomposed into a gradient force $\vec{F}_{\mathrm{g}} \propto \mathrm{Re}\{\alpha_{\mathrm{e}}\}\nabla|\vec{E}|^2$ and a radiation pressure force $\vec{F}_{\mathrm{p}} \propto \mathrm{Im}\{\alpha_{\mathrm{e}}\}\langle \vec{E} \times \vec{H}^* \rangle$ [43]. The radiation pressure does not change sign when crossing the focus of the beam, that is, it is always directed in the propagation direction for particles on-axis. The gradient force on the other hand changes sign since it always aligns with the direction of increasing intensity (for $\mathrm{Re}\{\alpha_{\mathrm{e}}\} > 0$). We thus decompose the total optical force acting on the particle into its symmetric and anti-symmetric parts [Fig. 2(b)] with respect to the focus position ($z = 0$) and identify the symmetric part as the radiation pressure force. Even though the term "gradient force" is traditionally associated with the electric dipole and paraxial field approximations, we borrow this expression and identify the anti-symmetric force part as such. The Fourier treatment recently presented in [44, 45] generalizes this decomposition to all of space, albeit in a numerically more demanding fashion.

In order to investigate the dipolar interference effects, we isolate the contributions to the optical force stemming from the different multipolar contributions in the same manner as in Fig. 1(c). This allows us to identify the contributions to the gradient and radiation pressure forces due to the electric (*ed*) and magnetic (*md*) dipole excitations of the sphere. As shown in Fig. 2(c), the *ed* and *md* contributions to the gradient force turn out to be completely additive, demonstrating

Optics EXPRESS

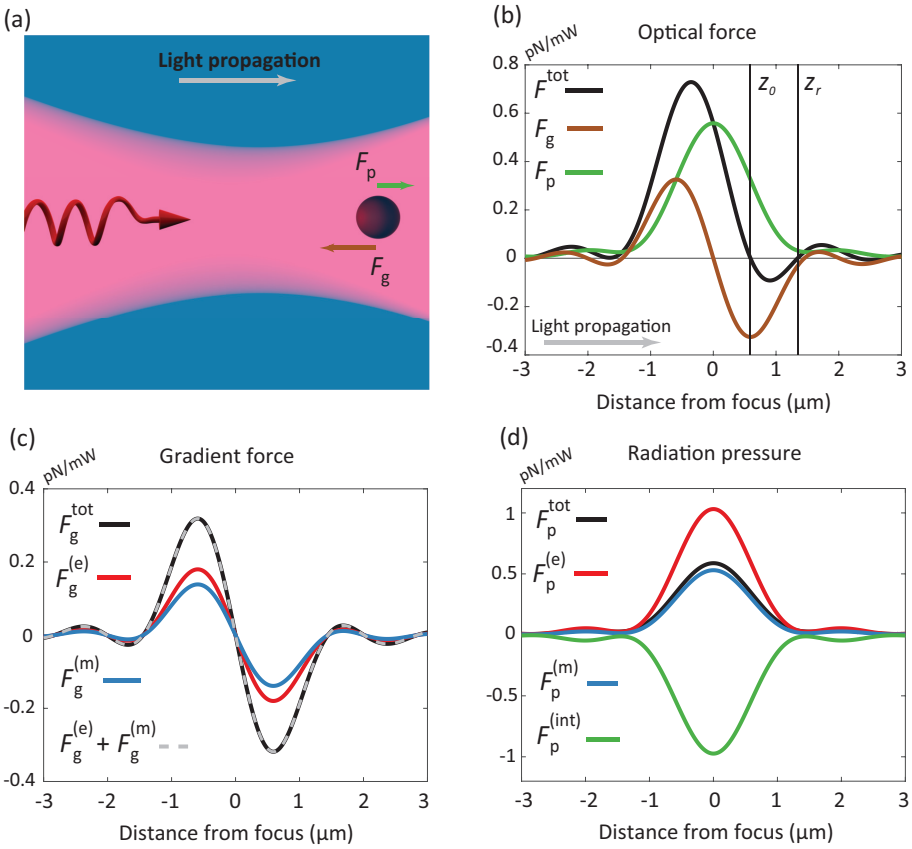

Fig. 2. Optical forces on a silicon sphere in a focused laser beam. Optical force simulations of a Si sphere with radius $r^* = 124.8$ nm (size parameter $x^* = 0.737$) situated in water and illuminated by a circularly polarized laser beam with wavelength $\lambda = 1064$ nm focused by a lens with numerical aperture NA = 1.2. The chosen sphere radius corresponds to the most stable trap situation for this set of illumination parameters. (a) Schematic of the simulated system. (b) The optical force in the direction of the optical axis (z) normalized to incident power. The total force (black) is decomposed into its symmetric (green) and anti-symmetric (brown) parts, which we identify as the radiation pressure F_p, and the gradient force F_g, respectively. (c) The gradient force contributions from all multipoles (black), from only the electric dipole (red) and from only the magnetic dipole (blue). The gray dashed line, which shows the sum of the two dipolar contributions, perfectly overlaps with the black line. This demonstrates that the gradient force is strictly additive, i.e. there are no interference effects. (d) The radiation pressure from all multipoles (black), from only the electric dipole (red) and from only the magnetic dipole (blue). The green line shows the difference $F_p^{(int)} = F_p^{tot} - F_p^{(e)} - F_p^{(m)}$ and demonstrates that interference between the induced electric and magnetic dipoles significantly reduces the radiation pressure. We note that the response for this particular size parameter is completely determined by the electric and magnetic dipole responses [c.f. Fig. 1(c)].

that no interference effects affect the gradient force in the present case despite the significant spectral and spatial overlap between the two modes. This is expected since the gradient force is caused by the fact that the potential energy of a particle is lowered if it has an induced (in-phase) electric dipole moment and moves towards a stronger electric field, or an induced magnetic dipole moment and moves towards a stronger magnetic field. In contrast, the radiation pressure exhibits

Optics EXPRESS

a clear interference effect analogous to the plane wave case, which can be seen by comparing the amplitude of total radiation pressure force with the two dipole contributions [Fig. 2(d), note that higher order multipoles have negligible effect for this parameter set]. The interference force, $F_{\mathrm{p}}^{(\mathrm{int})} = F_{\mathrm{p}}^{\mathrm{tot}} - (F_{\mathrm{p}}^{(\mathrm{e})} + F_{\mathrm{p}}^{(\mathrm{m})})$ is in fact almost as large as the electric dipole contribution, resulting in $F_{\mathrm{p}}^{\mathrm{tot}} \approx F_{\mathrm{p}}^{(\mathrm{m})}$.

Based on the analysis above, we now turn to the size dependence of the trap stability and the optical forces [Fig. 3]. Specifically, we investigate which sizes of silicon particles that can be stably trapped for the chosen trapping wavelength, numerical aperture and trapping medium, and how the different contributions to the optical forces influence the axial trapping potential.

The total optical force acting on the particle is non-conservative, and a potential energy can in principle not be defined. However, if we limit our analysis to axial forces acting on a particle on the optical axis, we can define an effective potential depth according to

$$W = \int_{z_0}^{z_{\mathrm{r}}} F_z \, \mathrm{d}z \,, \tag{3}$$

where z_0 and z_{r} are the axial positions where the optical force changes sign [shown in Fig. 2(b)]. Thus, z_0 corresponds to a local minimum in the potential energy (the particle's equilibrium position within the trap) and z_{r} corresponds to where the force becomes repulsive. W thus corresponds to the work required to move the particle along z from its equilibrium position to a point where it will be repelled [Fig. 3(a)]. This will be a good measure of the three-dimensional trap stability since the lateral restoring forces are much stronger than the axial forces for a single beam trap. It should also be mentioned that for certain parameter values, there exist multiple potential wells along the optical axis. In such cases, we selected the deepest well, usually the one closest to the beam focus. Figure 3(a) shows W/P_{in} expressed in units of $k_B T$ at room-temperature, $T = 293.15$ K. In order for an optical potential well to stably prevent the particle escaping through Brownian fluctuations, one typically estimates that the potential barrier

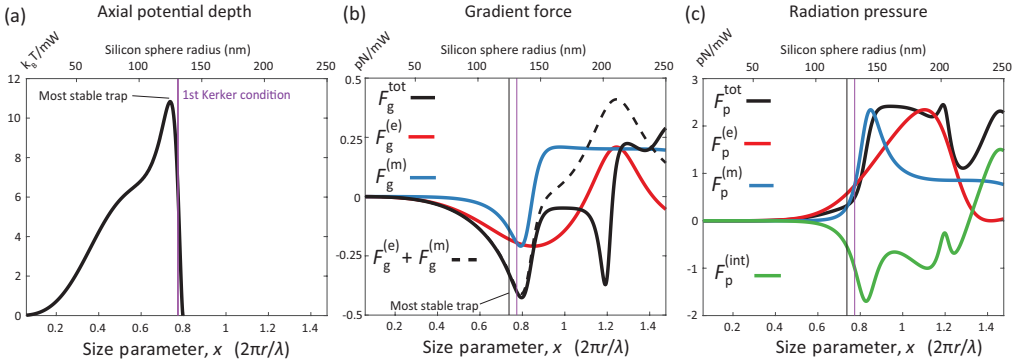

Fig. 3. Trap stability and optical force contributions versus particle size for silicon spheres in water. (a) Axial potential depth normalized to incident laser power, W/P_{in}, in units of $k_B T$ with $T = 293.15$ K. (b) Gradient force with all multipoles present (solid black line) and with only the electric dipole (red) or the magnetic dipole (blue) included in the calculation. The black dashed line shows the sum of the two dipolar contributions. Note that the gradient force components change sign upon crossing their respective resonance wavelengths. (c) Radiation pressure force from all multipoles (black) and from only the electric (red) or magnetic (blue) dipoles. The green line shows the dipole-dipole interference contribution $F_{\mathrm{p}}^{(\mathrm{int})} = F_{\mathrm{p}}^{\mathrm{tot}} - F_{\mathrm{p}}^{(\mathrm{e})} - F_{\mathrm{p}}^{(\mathrm{m})}$. The forces in (a) and (b) were calculated at $z = 600$ nm from the focus, where the gradient force is at its strongest [c.f. Fig. 2]. All calculations were performed for $\lambda = 1064$ nm, NA = 1.2 and circular polarization.

Optics EXPRESS

should exceed 10 k_BT [46] (under the assumption that light-induced heating can be neglected).

As seen in Fig. 3(a), the axial potential depth spectrum peaks at a size parameter of $x^* = 0.737$ (corresponding to $r^* = 124.8$ nm) while the first Kerker condition occurs at $x_k = 0.776$ ($r_k = 131$ nm). For even larger x, the trap becomes unstable (W undefined), meaning that trapping becomes impossible for any incident power. We again note that there is no discontinuity or other particular spectral feature associated with the first Kerker condition.

The dielectric particles widely employed in optical trapping generally have much lower refractive index than the Si particles considered here. It is therefore instructive to compare the present trap stability results in Fig. 3(a) with the trap stability for a particle made of e.g. polystyrene ($n \approx 1.57$). We also performed the same type of trap stability calculations for such spheres. In the size regime where the Si particles could be trapped (up to $r \sim 130$ nm), the trap stability for Si was found to be higher by a factor of 3 – 6. One can note that this factor is consistent with a rough estimate provided by forming the ratio $\alpha_{Si}/\alpha_{PS} \approx 6$ at $\lambda = 1064$ nm, using the corresponding simple Clausius-Mossotti electric dipole polarizabilities $\alpha = (n^2_{sphere} - n^2_s)/(n^2_{sphere} + 2n^2_s)$.

In the same manner as in Fig. 2, we now decompose the optical force into its symmetric and anti-symmetric parts, corresponding to the gradient [Fig. 3(b)] and radiation pressure [Fig. 3(c)] forces, respectively. In addition, we isolate the *ed* and *md* contributions to these forces by only keeping those corresponding multipolar response coefficients non-zero in the force calculation. We note that the magnetic gradient force, $F_g^{(m)}$, changes sign upon crossing the magnetic dipolar resonance [c.f. Fig. 1(a)], as is expected due to the real part of the magnetic dipole polarizability changing sign. In the same size region, we observe an increased radiation pressure stemming from the resonant scattering due to both electric and magnetic dipole resonances. These two effects combined serve to decrease the trap stability to a point where axial particle confinement is no longer possible at this numerical aperture and laser wavelength. The negative contribution to the radiation pressure due to the interference between electric and magnetic dipoles, $F_p^{(int)}$, is not enough to allow trapping of larger particles.

We also performed calculations of optical forces for silicon spheres for varying numerical aperture to investigate whether lower or higher focusing increases the importance of asymmetric scattering and the Kerker condition (not shown). We did not observe any appreciable effect of lower focusing, that is, by approaching the plane-wave case. In fact, the radiation pattern for a silicon sphere fulfilling the first Kerker condition ($r_k = 131$ nm at $\lambda = 1064$ nm) in the focused beam at $z = 600$ nm (NA = 1.2) is essentially identical to the radiation pattern in a plane wave (not shown). Thus, the only effect of lower focusing is a reduction in the restoring gradient forces and a corresponding weakening of the optical potential.

From our analysis, we can conclude that the most stable trapping is not directly related to the first Kerker condition. Rather, the trap becomes unstable at the onset of the particles' multipolar Mie resonances and the first Kerker condition also occurs at particle sizes in this region.

2.3. Optical forces on non-spherical silicon particles

Recent studies show that optimal forward-to-backward scattering is obtained for spheroidal shapes rather than spheres due to their better overlap between electric and magnetic dipole resonances [36, 37]. Since the interference force in the radiation pressure ($F_p^{(int)}$) stems from asymmetric scattering, we calculated the optical forces and optical potential depth for spheroidal silicon particles [Fig. 4] in order to further investigate the correspondence between asymmetric scattering and trap strength. The calculations were performed with a similar method as for the spherical particles. An incident focused (NA = 1.2) Gaussian laser beam with $\lambda = 1064$ nm was used and we employed the T-matrix method outlined in [39]. For a cylindrically symmetric particle (e.g. spheroid) aligned along the z-axis, the T-matrix is diagonal in the quantum number m but couples multipole orders corresponding to different ℓ. This is in contrast to the spherical

Optics EXPRESS

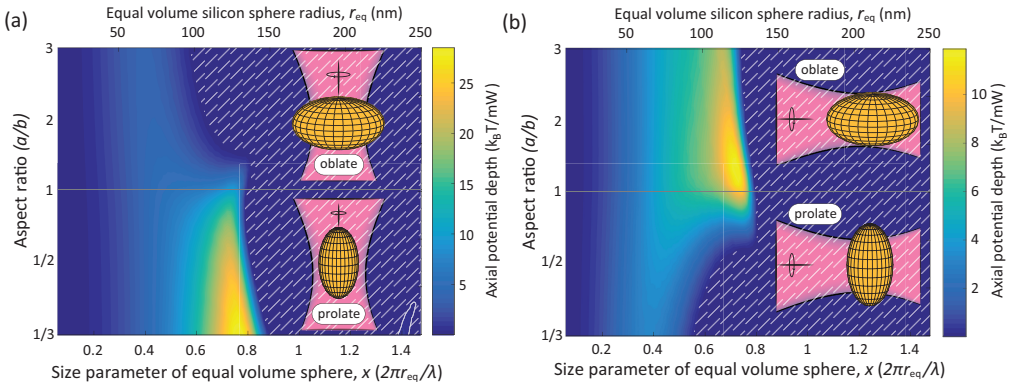

Fig. 4. Trap stability for spheroidal silicon particles in water. The axial potential depth normalized to the incident power for spheroids with different aspect ratios a/b, where b is the half-axis along the spheroid symmetry axis. Thus, for aspect ratios > 1 (< 1) we have oblate (prolate) spheroids. The excitation is $\lambda = 1064$ nm in water. The particles considered here have the same volume as the spheres considered in Fig. 1(a) and the size is therefore shown as the radius of a sphere with that volume for ease of comparison. (a) The potential depth for incidence along the spheroid symmetry axis. (b) The potential depth for incidence 90 tilted from the spheroid symmetry axis. The regions with gray dashed lines correspond to parameter values where there is no axial potential well, making trapping impossible. We see that by changing the shape of the particles, there is no drastic gain in terms of being able to trap particles with higher volume.

case (standard Mie theory) where the T-matrix is completely diagonal. Using this T-matrix, the electromagnetic fields and the Maxwell stress tensor were calculated on the circumscribing sphere, S_c. From this, we proceeded the same way as for the spherical particles in calculating the optical forces.

We performed calculations for different aspect ratios (a/b), where a and b are the half-axes of the spheroidal particle. We chose b to be the half-axis along the spheroid symmetry axis, such that $a > b$ is an oblate spheroid and $a < b$ is a prolate spheroid. In order to compare the trapping efficiency with the spherical particles studied previously, we introduce an "equal volume sphere radius" r_{eq} such that $a^2 b = r_{eq}^3$. This allows for investigation of whether or not particles of larger volume can be trapped through deformation of a sphere.

Both incidence along and perpendicular to the spheroid symmetry axis was considered. For the case where the particle symmetry axis was not aligned with the z-axis in space, we still exploited the cylindrical symmetry of the particle by Wigner rotating the multipole expansion of the incident field to the particle frame. The force was then calculated in that frame and subsequently transformed back. For light incident parallel to the spheroid symmetry axis, that is when the maximum geometric cross section for oblate spheroids and the minimum for prolate spheroids face the wave front [Fig. 4(a)], the axial potential is deeper and thus trapping requires lower laser powers for prolate shapes. This is in contrast to the increased forward-to-backward scattering observed for oblate spheroids [36], indicating that the increased area exposed to the beam, and the concomitant increase in resonant radiation pressure has a more pronounced effect on the trap stability than the scattering asymmetry has. The same effect is observed for light incident perpendicular to the spheroid symmetry axis [Fig. 4(b)]. In this case, the trap is more stable for the oblate spheroids due to a smaller area being exposed to the beam for oblate shapes.

For both directions of incidence, there can be a small gain in particle volume compared to spherical shapes, but not more than ~ 20 nm in equivalent radius. One exception to this was observed for highly prolate spheroids and incidence along the symmetry axis [bottom right, Fig.

Optics EXPRESS

4(a)]. There is a small region in which trapping is possible for equal sphere radii around 240 nm. However, the axial potential is shallow and stable trapping ($\sim 10\, k_B T$) would require laser powers around 100 mW at room temperature.

3. Summary and conclusions

We have demonstrated that small silicon particles ($r < \sim 130$ nm) can be stably trapped in three dimensions at a wavelength of $\lambda = 1064$ nm. Stable trapping of particles as small as $r = 50$ nm requires modest laser powers of ~ 5 mW and due to the low silicon absorption at this wavelength, photothermal heating is negligible. Moreover, the precise shape of the particles (spherical or elongated), does not drastically change the particle volumes able to be trapped.

Silicon particles support both electric and magnetic dipole polarizabilities that both contribute to the radiation pressure force and gradient force. We have isolated the different multipolar contributions to these forces and determined that the main factor determining the trap stability is not the asymmetric scattering by multipolar interference, but rather the sharply increasing resonant radiation pressure for larger particle sizes. Additionally, the magnetic gradient force changes sign as the magnetic resonance approaches the excitation wavelength and becomes repulsive, further weakening the trap. The first Kerker condition, while constituting the optimal angular scattering distribution in terms of minimizing radiation pressure, does not correspond to the most stable trap.

Optical trapping and manipulation of small particles have many potential uses in biotechnology and biomedicine, and the advantage in such applications of using silicon particles over, say, metallic particles is the drastically reduced photothermal heating. It should be noted that while the absorption of silicon is negligible for our chosen wavelength of $\lambda = 1064$ nm, this is not the case for other common optical trapping wavelengths at higher photon energies. In such cases, the photo-induced thermal effects on the particle dynamics will need to be taken into account.

Funding

Swedish Foundation for Strategic Research (SSF) (project number RMA11-0037); The Knut and Alice Wallenberg Foundation.

Acknowledgments

We would like to thank S. Jones, P. Karpinski, H. Šípová and R. Verre for stimulating discussions.

References

1. A. Ashkin, "Acceleration and Trapping of Particles by Radiation Pressure," Phys. Rev. Lett. **24**, 156–159 (1970).
2. P. C. Ashok and K. Dholakia, "Optical trapping for analytical biotechnology," Curr. Opin. Biotechnol. **23**, 16–21 (2012).
3. F. M. Fazal and S. M. Block, "Optical tweezers study life under tension," Nat. Photonics **5**, 318 – 321 (2011).
4. A. Lehmuskero, P. Johansson, H. Rubinsztein-Dunlop, L. Tong, and M. Käll, "Laser Trapping of Colloidal Metal Nanoparticles," ACS Nano **9**, 3453–3469 (2015).
5. P. Lebel, A. Basu, F. C. Oberstrass, E. M. Tretter, and Z. Bryant, "Gold rotor bead tracking for high-speed measurements of DNA twist, torque and extension," Nat. Methods **11**, 456–462 (2014).
6. M. Li, T. Lohmüller, and J. Feldmann, "Optical Injection of Gold Nanoparticles into Living Cells," Nano Lett. **15**, 770–775 (2015).
7. D. Boyer, P. Tamarat, A. Maali, B. Lounis, and M. Orrit, "Photothermal imaging of nanometer-sized metal particles among scatterers." Science **297**, 1160–1163 (2002).
8. M. Fedoruk, M. Meixner, S. Carretero-Palacios, T. Lohmüller, and J. Feldmann, "Nanolithography by Plasmonic Heating and Optical Manipulation of Gold Nanoparticles," ACS Nano **7**, 7648–7653 (2013).
9. D. Rings, R. Schachoff, M. Selmke, F. Cichos, and K. Kroy, "Hot Brownian Motion," Phys. Rev. Lett. **105**, 090604 (2010).
10. A. Lehmuskero, R. Ogier, T. Gschneidtner, P. Johansson, and M. Käll, "Ultrafast Spinning of Gold Nanoparticles in Water Using Circularly Polarized Light," Nano Lett. **13**, 3129–3134 (2013).

Optics EXPRESS

11. Z. Yan, J. E. Jureller, J. Sweet, M. J. Guffey, M. Pelton, and N. F. Scherer, "Three-Dimensional Optical Trapping and Manipulation of Single Silver Nanowires," Nano Lett. **12**, 5155–5161 (2012).
12. D. Lin, P. Fan, E. Hasman, and M. L. Brongersma, "Dielectric gradient metasurface optical elements," Science **345**, 298–302 (2014).
13. M. Decker, I. Staude, M. Falkner, J. Dominguez, D. N. Neshev, I. Brener, T. Pertsch, and Y. S. Kivshar, "High-Efficiency Dielectric Huygens' Surfaces," Adv. Opt. Mater. **3**, 813–820 (2015).
14. A. I. Kuznetsov, A. E. Miroshnichenko, M. L. Brongersma, Y. S. Kivshar, and B. Luk'yanchuk, "Optically resonant dielectric nanostructures," Science **354**, aag2472 (2016).
15. L. Cao, J. S. White, J.-S. Park, J. A. Schuller, B. M. Clemens, and M. L. Brongersma, "Engineering light absorption in semiconductor nanowire devices," Nat. Mater. **8**, 643–647 (2009).
16. P. Spinelli, M. Verschuuren, and A. Polman, "Broadband omnidirectional antireflection coating based on subwavelength surface Mie resonators," Nat. Commun. **3**, 692 (2012).
17. L. Cao, P. Fan, A. P. Vasudev, J. S. White, Z. Yu, W. Cai, J. A. Schuller, S. Fan, and M. L. Brongersma, "Semiconductor Nanowire Optical Antenna Solar Absorbers," Nano Lett. **10**, 439–445 (2010).
18. Q. Zhao, J. Zhou, F. Zhang, and D. Lippens, "Mie resonance-based dielectric metamaterials," Mater. Today **12**, 60–69 (2009).
19. A. B. Evlyukhin, C. Reinhardt, A. Seidel, B. S. Luk'Yanchuk, and B. N. Chichkov, "Optical response features of Si-nanoparticle arrays," Phys. Rev. B **82**, 045404 (2010).
20. D. A. Shilkin, E. V. Lyubin, M. R. Shcherbakov, M. Lapine, and A. A. Fedyanin, "Directional Optical Sorting of Silicon Nanoparticles," ACS Photonics **4**, 2312–2319 (2017).
21. T.-a. Yano, Y. Tsuchimoto, R. P. Zaccaria, A. Toma, A. Portela, and M. Hara, "Enhanced optical magnetism for reversed optical binding forces between silicon nanoparticles in the visible region," Opt. Express **25**, 431–439 (2017).
22. A. Andres-Arroyo, B. Gupta, F. Wang, J. J. Gooding, and P. J. Reece, "Optical Manipulation and Spectroscopy Of Silicon Nanoparticles Exhibiting Dielectric Resonances," Nano Lett. **16**, 1903–1910 (2016).
23. R. Paniagua-Domínguez, Y. F. Yu, A. E. Miroshnichenko, L. A. Krivitsky, Y. H. Fu, V. Valuckas, L. Gonzaga, Y. T. Toh, A. Y. S. Kay, B. Luk'yanchuk, and A. I. Kuznetsov, "Generalized Brewster effect in dielectric metasurfaces," Nat. Commun. **7**, 10362 (2016).
24. J. Geffrin, B. García-Cámara, R. Gómez-Medina, P. Albella, L. Froufe-Pérez, C. Eyraud, A. Litman, R. Vaillon, F. González, M. Nieto-Vesperinas, J. Sáenz, and F. Moreno, "Magnetic and electric coherence in forward- and back-scattered electromagnetic waves by a single dielectric subwavelength sphere," Nat. Commun. **3**, 1171 (2012).
25. C. Pfeiffer and A. Grbic, "Metamaterial Huygens' surfaces: Tailoring wave fronts with reflectionless sheets," Phys. Rev. Lett. **110**, 197401 (2013).
26. M. Kerker, D.-S. Wang, and C. L. Giles, "Electromagnetic scattering by magnetic spheres," J. Opt. Soc. Am. **73**, 765–767 (1983).
27. Y. H. Fu, A. I. Kuznetsov, A. E. Miroshnichenko, Y. F. Yu, and B. Luk'yanchuk, "Directional visible light scattering by silicon nanoparticles," Nat. Commun. **4**, 1527 (2013).
28. J. J. Sáenz, "Laser tractor beams," Nat. Photonics **5**, 514–515 (2011).
29. J. Chen, J. Ng, Z. Lin, and C. T. Chan, "Optical pulling force," Nat. Photonics **5**, 531–534 (2011).
30. W. Liu, "Generalized Magnetic Mirrors," Phys. Rev. Lett. **119**, 123902 (2017).
31. S. Sukhov and A. Dogariu, "Non-conservative optical forces," Reports on Prog. Phys. **80**, 112001 (2017).
32. M. Nieto-Vesperinas, R. Gomez-Medina, and J. J. Saenz, "Angle-suppressed scattering and optical forces on submicrometer dielectric particles," J. Opt. Soc. Am. A **28**, 54–60 (2011).
33. R. Gómez-Medina, L. S. Froufe-Pérez, M. Yépez, F. Scheffold, M. Nieto-Vesperinas, and J. J. Sáenz, "Negative scattering asymmetry parameter for dipolar particles: Unusual reduction of the transport mean free path and radiation pressure," Phys. Rev. A **85**, 035802 (2012).
34. A. B. Stilgoe, T. A. Nieminen, G. Knöner, N. R. Heckenberg, and H. Rubinsztein-Dunlop, "The effect of Mie resonances on trapping in optical tweezers," Opt. Express **16**, 15039–15051 (2008).
35. S. H. Simpson and S. Hanna, "Computational study of the optical trapping of ellipsoidal particles," Phys. Rev. A **84**, 053808 (2011).
36. B. S. Luk'yanchuk, N. V. Voshchinnikov, R. Paniagua-Domínguez, and A. I. Kuznetsov, "Optimum Forward Light Scattering by Spherical and Spheroidal Dielectric Nanoparticles with High Refractive Index," ACS Photonics **2**, 993–999 (2015).
37. Z. Wang, N. An, F. Shen, H. Zhou, Y. Sun, Z. Jiang, Y. Han, Y. Li, and Z. Guo, "Enhanced Forward Scattering of Ellipsoidal Dielectric Nanoparticles," Nanoscale research letters **12**, 58 (2017).
38. L. Novotny and B. Hecht, *Principles of nano-optics* (Cambridge University, 2012).
39. P. C. Waterman, "Symmetry, Unitarity, and Geometry in Electromagnetic Scattering," Phys. Rev. D **3**, 825–839 (1971).
40. J. P. Barton, D. R. Alexander, and S. A. Schaub, "Theoretical determination of net radiation force and torque for a spherical particle illuminated by a focused laser beam," J. Appl. Phys. **66**, 4594–4602 (1989).
41. V. D. Miljković, T. Pakizeh, B. Sepulveda, P. Johansson, and M. Käll, "Optical Forces in Plasmonic Nanoparticle Dimers," The J. Phys. Chem. C **114**, 7472–7479 (2010).
42. M. A. Green, "Self-consistent optical parameters of intrinsic silicon at 300 K including temperature coefficients," Sol. Energy Mater. Sol. Cells **92**, 1305–1310 (2008).

Optics EXPRESS

43. M. Nieto-Vesperinas, J. J. Sáenz, R. Gómez-Medina, and L. Chantada, "Optical forces on small magnetodielectric particles," Opt. Express **18**, 11428–11443 (2010).
44. J. Du, C.-H. Yuen, X. Li, K. Ding, G. Du, Z. Lin, C. T. Chan, and J. Ng, "Tailoring Optical Gradient Force and Optical Scattering and Absorption Force," Sci. Reports **7**, 18042 (2017).
45. J. Chen, K. Li, and X. Li, "Influence of permittivity on gradient force exerted on Mie spheres," J. Opt. Soc. Am. A **35**, 553–560 (2018).
46. Y. Harada and T. Asakura, "Radiation forces on a dielectric sphere in the Rayleigh scattering regime," Opt. Commun. **124**, 529–541 (1996).